BIOCHEMISTRY
including biophysical chemistry & molecular biology

Article

pubs.acs.org/biochemistry

Conformational Changes of the Antibacterial Peptide ATP Binding Cassette Transporter McjD Revealed by Molecular Dynamics Simulations

Ruo-Xu Gu,[†] Valentina Corradi,[†] Gurpreet Singh,[†] Hassanul G. Choudhury,[‡,§,∥,#] Konstantinos Beis,[‡,§,∥] and D. Peter Tieleman*[,†]

[†]Centre for Molecular Simulation and Department of Biological Sciences, University of Calgary, 2500 University Drive, N.W., Calgary, Alberta T2N 1N4, Canada

[‡]Department of Life Sciences, Imperial College London, South Kensington, London SW7 2AZ, United Kingdom

[§]Membrane Protein Lab, Diamond Light Source, Harwell Science and Innovation Campus, Oxfordshire, OX11 0DE, United Kingdom

[∥]Rutherford Appleton Laboratory, Research Complex at Harwell, Oxfordshire OX11 0DE, United Kingdom

Supporting Information

ABSTRACT: The ATP binding cassette (ABC) transporters form one of the largest protein superfamilies. They use the energy of ATP hydrolysis to transport chemically diverse ligands across membranes. An alternating access mechanism in which the transporter switches between inward- and outward-facing conformations has been proposed to describe the translocation process. One of the main open questions in this process is the degree of opening of the transporter at different stages of the transport cycle, as crystal structures and biochemical data have suggested a wide range of distances between nucleotide binding domains. Recently, the crystal structure of McjD, an antibacterial peptide ABC transporter from *Escherichia coli*, revealed a new occluded intermediate state of the transport cycle. The transmembrane domain is closed on both sides of the membrane, forming a cavity that can accommodate its ligand, MccJ25, a lasso peptide of 21 amino acids. In this work, we investigate the degree of opening of the transmembrane cavity required for ligand translocation. By means of steered molecular dynamics simulations, the ligand was pulled from the internal cavity to the extracellular side. This resulted in an outward-facing state. Comparison with existing outward-facing crystal structures shows a smaller degree of opening in the simulations, suggesting that the large conformational changes in some crystal structures may not be necessary even for a large substrate like MccJ25.

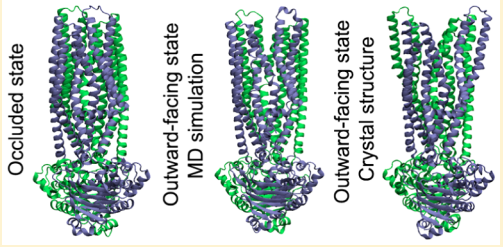

INTRODUCTION

ABC transporters constitute one of the largest protein superfamilies. They transport ligands of diverse chemical properties, from ions to lipids, sterols, and peptides, across membranes.[1] They are widely distributed in all kingdoms of life, and are involved in numerous physiological processes, including the import of antigen peptides into the lumen of endoplasmic reticulum,[2] lipid translocation, and assembly of high-density lipoproteins.[3] Thus, mutations in ABC transporters are often associated with diseases (e.g., diabetes and cystic fibrosis),[4,5] while an increased expression of several members of this superfamily is one of the primary causes of multidrug resistance.[6,7]

ABC transporters couple the transport of their substrates with the binding and hydrolysis of ATP. Bacterial ABC exporters typically exist as dimers. Each monomer contains an N-terminal transmembrane domain (TMD) consisting of six transmembrane (TM) helices that form the translocation pathway for ligand binding and export, and a C-terminal nucleotide-binding domain (NBD) that binds and hydrolyzes ATP. The ATP binding sites are located at the interfacial region of the two NBDs, whose dimerization and dissociation induced by ATP binding and hydrolysis are coupled to conformational changes of the TMDs.

An alternating access mechanism has been proposed for the translocation process, in which the transporter switches from an inward-facing to an outward-facing state.[8−10] The inward-facing state is characterized by the ligand-binding cavity being accessible from the cytoplasmic side, while different degrees of separation have been observed for the NBDs. Binding of ATP molecules induces dimerization of the NBDs as well as conformational changes in the TMDs in such a way that the ligand-binding cavity becomes accessible to the extracellular side. The conformation reverts to the inward-facing state after the hydrolysis of the ATP molecules. We have shown that the transition from an outward- to inward-facing conformation may

Received: July 6, 2015
Revised: August 28, 2015
Published: September 3, 2015

DOI: 10.1021/acs.biochem.5b00753
Biochemistry 2015, 54, 5989−5998

occur via an occluded state.[8] We also hypothesized that an occluded transition state will occur during the transition from an inward- to an outward-facing conformation.

In addition to crystallographic studies, molecular dynamics simulations have been extensively used to investigate the mechanism of ABC exporters.[11−25] While equilibrium methods are usually applied to study the properties of a given conformational state, nonequilibrium approaches can been used to characterize possible pathways from one conformational state to another. In the case of ABC transporters, nonequilibrium methods allowed to investigate possible transitions between crystal structures representing possible inward-facing and outward-facing states of a given transporter, notably MsbA,[15,24] which has been crystallized in a number of different conformations.

The crystal structure of the ABC transporter McjD from *E. coli* adopts an occluded conformation[8] in the absence of a ligand that has not been observed before. McjD is essential for resistance to cells that synthesize the antibacterial peptide, Microcin J25 (MccJ25), a 21 amino acids post-translationally modified peptide that adopts a lasso structure.[26] Unlike other ABC transporters, McjD defines a binding cavity of ∼5900 Å^3 that is occluded from both sides of the membrane. This cavity can accommodate one MccJ25 molecule (Figure 1).[8] We have

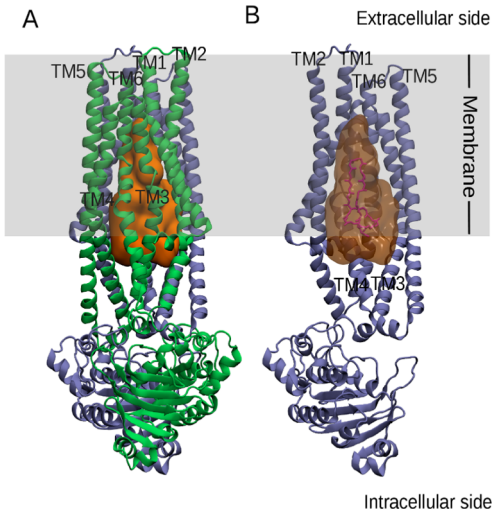

Figure 1. MccJ25 binding cavity in the McjD transporter. In Panel A, the two chains of McjD are shown in green and blue, respectively, whereas the surface of the ligand binding cavity in the transporter is shown in orange. In Panel B, only one chain of the protein is shown for clarity. MccJ25 manually docked in McjD is shown in magenta. The surface of ligand binding cavity is shown in transparent model. The position of the bilayer is shown in gray.

previously reported a possible model for the MccJ25 position within the McjD cavity and evaluated it by site-direct mutagenesis, ligand induced ATPase activity and ligand binding assays.[8]

Here, we apply nonequilibrium simulation methods to investigate the degree of opening of the McjD transporter while switching from the crystallographically determined occluded state to a putative outward-facing state. While previous nonequilibrium studies used conformational states of crystal structures as initial and final states,[15,24] in our work we investigate the opening of the TMDs as a consequence of ligand translocation. Starting from an initial model of the orientation of MccJ25 in the occluded cavity,[8] we conducted steered molecular dynamics (MD) simulations to promote the release of the ligand to the extracellular side. The transporter switched to an outward-facing conformation after ligand release. However, the conformational changes we observed are smaller than those suggested by available outward-facing crystal structures.[9,10]

METHODS

McjD-MccJ25 Model. As a starting structure for the steered MD simulations, we used the McjD-MccJ25 complex (Figure 1) suggested by Choudhury et al.[8] The NMR structure of MccJ25 (PDB ID: 1Q71)[27] was positioned inside the McjD cavity (PDB ID: 4PL0) based on minimum steric clashes and possible bonds with McjD.[8] The substrate is too large and flexible to be confident of an accurate docking pose, and more computationally intensive docking methods are not likely to identify better docking poses. For the purpose of the simulations in this study this is not essential, but it precludes detailed analyses of interactions between specific residues of the substrate with specific residues of the transporter.

The McjD crystal structure was determined in complex with the ATP analogue AMP-PNP, which was replaced with ATP molecules in our simulations.

Molecular Dynamics Simulations. The simulations were conducted using the GROMACS package.[28,29] The AMBER99S-ILDN force field[30] and the slipids force field[31−33] were used to describe protein and lipids, respectively, while ATP parameters were from Meagher et al.[34] Standard protonation states defined in GROMACS were used for the titratable residues. A cutoff distance of 1.0 nm was used for the van der Waals interactions, whereas long-range electrostatic interactions were calculated by the PME algorithm.[35,36] The temperature and the pressure were maintained at 310 K and 1 atm by velocity rescaling[37] and Parrinello−Rahman pressure coupling,[38,39] respectively. Initially, the complex was inserted into a pre-equilibrated POPC bilayer[31] using the g_membed tool.[40] The system was solvated using TIP3P[41,42] water molecules, and Na^+ ions were added to neutralize the system. The size of the simulation box was about 12.5 nm × 13 nm × 20 nm.

Prior to steered MD simulations, 500 steps of minimization were conducted using the steepest descent algorithm, followed by another 500 steps by conjugate gradient algorithm to minimize the system. Twenty-five ns simulation with position restraints applied to the McjD-MccJ25 complex were conducted to equilibrate the lipids and solvent around the protein. Following this equilibration, multiple steered MD simulations were performed using different pullrates (ranging from 1×10^{-4} nm/ps to 4×10^{-6} nm/ps) and force constants (ranging from 500 kJ/(mol nm^2) to 3000 kJ/(mol nm^2)) to pull MccJ25 to the extracellular side along the Z direction, normal to the bilayer. The simulations are summarized in Table 1.

Homology Modeling. To compare the structural changes in McjD after the steered molecular dynamics to a known outward-facing structure, we built a homology model of McjD based on the outward-facing structure of the (remote) homologous bacterial protein Sav1866. The outward-facing model of McjD was obtained by following the same protocol described by Corradi et al. for homology models of TAP.[43] For the TMDs, the sequence of McjD was aligned to the sequences of homologous ABC transporters, namely human and rat TAP1

DOI: 10.1021/acs.biochem.5b00753
Biochemistry 2015, 54, 5989−5998

Table 1. Steered Molecular Dynamics Simulations Conducted in This Study[a]

	force constant (kJ/(mol nm^2))	pull rate (nm/ps)	length of simulation (ns)	initial conformation
Group 1	500 1000 1500 2000 2500 3000	1×10^{-4}	60	McjD−MccJ25 complex suggested by Choudhury et al.[8]
Group 2 repeated 6 times with different initial velocities referred to as Simulation 1−6	2000	4×10^{-5}	150	McjD−MccJ25 complex suggested by Choudhury et al.[8]
Group 3 repeated three times	2000	4×10^{-6}	500	snapshot at 50 ns extracted from Simulation 1 in Group 2
Group 4 system was equilibrated at each force maximum[b]	2000	4×10^{-5}	1560	McjD−MccJ25 complex suggested by Choudhury et al.[8]

[a]Four groups of simulations were performed using different parameters. [b]Equilibrated system for 150 ns before pull and equilibrated system for 150 ns at each force maximum with ligand restrained with force constants of 8000 kJ/(mol nm^2).

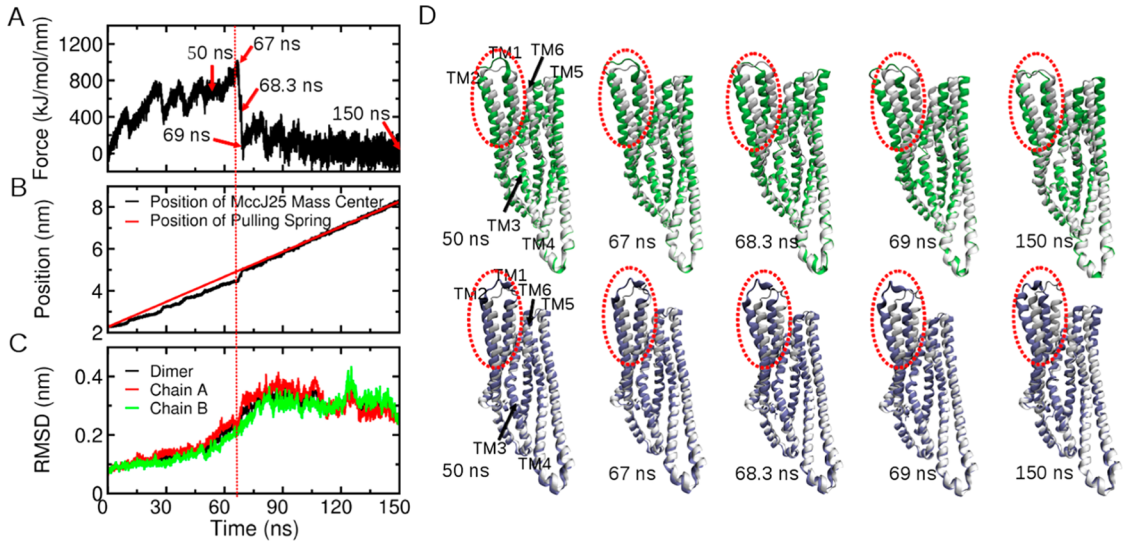

Figure 2. Conformational changes in McjD. (A) The pull force profile; (B) The positions of center of mass of MccJ25 relative to the protein; (C) RMSD values of TMDs relative to the occluded state; (D) Superimposition of snapshots of the trajectory with the initial occluded McjD structure. All panels are based on simulation 1 of Group 2 (Table 1). Only the TMDs are shown for clarity. Chain A and chain B of the snapshots of the trajectory are shown in green and blue, respectively, whereas both chains of the occluded McjD structure are shown in gray. RMSDs were calculated for each monomer based on fitting TM3−6 of both monomers to the initial dimer structure. The dashed red line marks the maximum pulling force.

and TAP2, human ABCB10, *E. coli* Sav1866, *T. maritima* TM287−288, and *V. cholera*, *E. coli* and *S. typhimurium* MsbA. For the NBDs, the alignment also included the sequences of *E. coli* hemolysin B, human ABCB6, and MRP2 from *P. yoelii*. The final alignments for TMDs and NBDs were generated using MAFFT (Figures S1−2).[44] The sequence identities between McjD and Sav1866 are 13% and 32% for the TMDs and NBDs, respectively.

The outward-facing homology model of McjD based on these alignments was built by means of MODELER 9v10[45] using the structure of Sav1866 as a template.[9] Twenty models were generated and the one with the best score in terms of the discrete optimized protein energy potential implemented in MODELER was chosen.

RESULTS

Effect of Force Constant and Pull Rate. Because steered molecular dynamics is a nonequilibrium technique, the results depend on the pull rate and possibly on the force constant used for the virtual spring that pulls the ligand. In the limit of very slow (infinitely slow) pulling and a reasonable choice of reaction coordinate, the simulations would give the thermodynamic work of moving the ligand, but in practice this is not achievable for a system of this complexity. This means that the calculated work, based on the pull force and displacement, includes a pull-rate dependent frictional component. In order to evaluate the effect of different force constants, we first conducted control simulations with six different force constants ranging from 500 to 3000 kJ/(mol nm^2) and a pull rate of 1×10^{-4} nm/ps (Simulations of Group 1 in Table 1). These simulations, of 60 ns each, resulted in comparable force profiles (Figures S3−4), associated with conformational changes of the

DOI: 10.1021/acs.biochem.5b00753
Biochemistry 2015, 54, 5989−5998

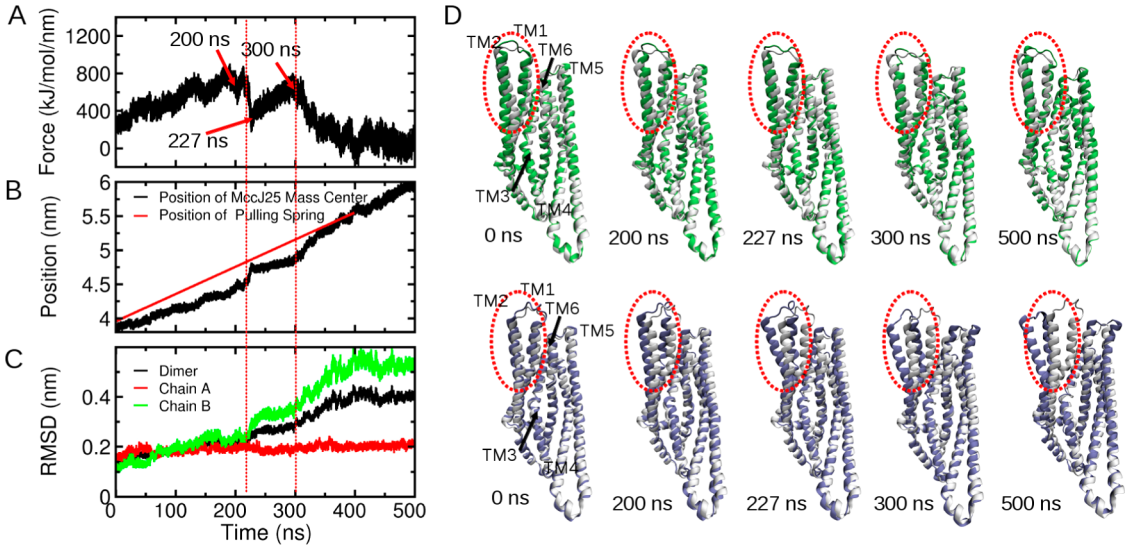

Figure 3. Conformational changes in McjD. (A) The pull force profile; (B) The positions of MccJ25 mass center relative to the protein; (C) RMSD values of TMDs relative to the occluded state; (D) Structural superimpositions of selected snapshots with the occluded structure. All panels are based on a simulation from Group 3 (Table 1). The protein structures are colored in the same way as in Figure 2. The dashed red line marks the maximum pulling force.

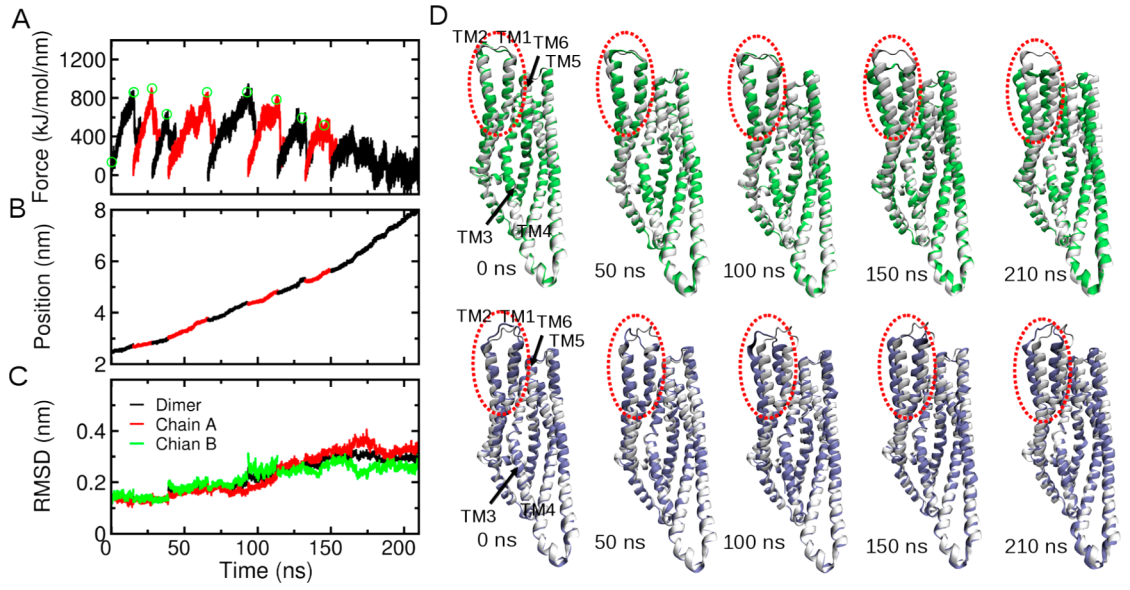

Figure 4. Conformational changes in McjD. (A) The pull force profile; (B) the positions of MccJ25 mass center relative to the protein; (C) RMSD values of TMDs relative to the occluded state; (D) structural superimpositions of selected snapshots with the occluded crystal structure. All panels are based on the simulation in Group 4 (Table 1). The protein structures are colored in the same way as in Figure 2.

TMDs of the transporter (Figure S5). However, when larger force constants are used (e.g., 3000 kJ/(mol nm^2)), more frictions were introduced between MccJ25 and McjD, as indicated by different fluctuations of the forces in Figure S3. Thus, for further simulations we used an intermediate force constant of 2000 kJ/(mol nm^2) (Figures 2, 3, and 4). The pull rates used are a compromise based on the available computer resources and the resulting time required for the simulations and an attempt to make the friction work as small as possible. They span a 25-fold range (see details in Table 1), with as slowest pull rate1 4×10^{-6}nm/ps, or 4 nm per microsecond of simulation time. At this slowest rate, the friction to pull the peptide in solution is negligible but this is not the case when pulling the peptide through the protein.

Different pulling rates and pulling force constants did not result in significant differences of the conformational changes of the NBDs and TMDs. The NBDs maintained a stable dimer structure in all the simulations. The averaged RMSD values for the backbone of the NBDs were in the range of 0.15−0.2 nm in most of the simulations of Group 1, 2, and 3 (Table 1) (the RMSD values were averaged over the last 40 ns, the last 100 ns, and the whole simulation time for Group 1, 2, and 3, respectively). The only exceptions were simulations 3 and 6 in Group 2, in which the average RMSD values were about 0.24 nm. In all the simulations, the TMDs showed larger conformational changes than the NBDs, as indicated by the RMSD values in Figure 2, 3, and 4. The conformational changes of the TMDs are discussed in detail in the following sections.

DOI: 10.1021/acs.biochem.5b00753
Biochemistry 2015, 54, 5989−5998

Conformational Changes during Translocation. We conducted 6 simulations with a pull rate of 4×10^{-5} nm/ps and a force constant of 2000 kJ/(mol nm^2) (simulations of Group 2 in Table 1, referred as Simulations 1−6 in this study) to confirm the reproducibility of our calculations. The force profiles in these simulations were quite similar (Figures 2A, S6A, S7A, and S8). The force reached a maximum of ∼1000 kJ/(mol nm) in ca. 75 ns and then rapidly dropped to ca. 300−400 kJ/(mol nm), to gradually decrease and fluctuate at around 0 kJ/(mol nm) during the last 20 ns. The shapes and maximum values of these force profiles are comparable with those obtained by using a larger pull rate and different force constants (Simulations of Group 1 in Table 1, Figure S3).

As shown in Figure 2C, the RMSD values of the TMDs of the protein increased from 0.1 to 0.3 nm between ca. 60 to 90 ns. Structure superimpositions of snapshots from the simulations with the occluded crystal structure show that conformational changes occurred at ca. 68 ns (Figure 2D). The pull force dropped from ∼1000 to ∼200 kJ/(mol nm) between ca. 67 to 69 ns (Figure 2A). This indicates that the conformational changes happened in a short time after the force reached its maximum value, followed by a rapid and significant decrease in the pull force values.

The large force detected during the first 60 ns implies steric hindrance between ligand and transporter due to the small volume of the transmembrane cavity (see Figure 1 for the cavity in the occluded structure). The transition to a state with a certain degree of opening on the extracellular side, associated with lower pull force values, indicates an increased cavity size and reduced steric hindrance between MccJ25 and McjD. The smaller pull force values that follow the protein conformational changes suggest that the extracellular opening of the TMDs should be large enough to allow ligand release. This relationship between the pull force decreasing values and the conformational changes were also observed in other simulations (Figures S6−8).

By comparing the outward-facing states obtained from the simulations with the occluded crystal structure, we observe (i) major changes for TM1 and 2, (ii) minor changes for TM5 and 6, and (iii) almost no changes for TM3 and 4 (Figure 2D). Similar conclusions can be obtained from the comparison of the McjD crystal structure with the outward-facing homology model of McjD built using the structure of Sav1866 as a template (Figure 5). In this model, TM1 and 2 are separated from TM3 and 6 of the same half, and interact with TM4 and 5 of the opposite subunit. While these structural changes were also revealed by analyses and comparisons of different crystal structures,[8−10,46] our MD simulations raise the possibility that the range of opening involving TM1 and TM2 is smaller than what is suggested by the McjD homology model based on Sav1866 (Figure 5).

To investigate the degree of extracellular opening in more detail, we calculated the distances between the two Leu53 residues (Figure 6). Leu53 is located at extracellular loop 1 (ECL1, the loop connecting TM1 and TM2). In the occluded state, Leu53 of each monomer interacts with the Leu53 of the opposite monomer,[8] whereas if the transporter adopts an outward-facing state, they will move away from each other and the distance between them will increase. Thus, the distance between these residues is a measure of the degree of transporter opening at the extracellular side. The distances between their centers of mass are 0.5, 2.6, and 1.5 nm for the occluded state, the outward-facing homology model and the outward-facing state extracted at the end of the MD simulation, respectively (Figure 6A-C).

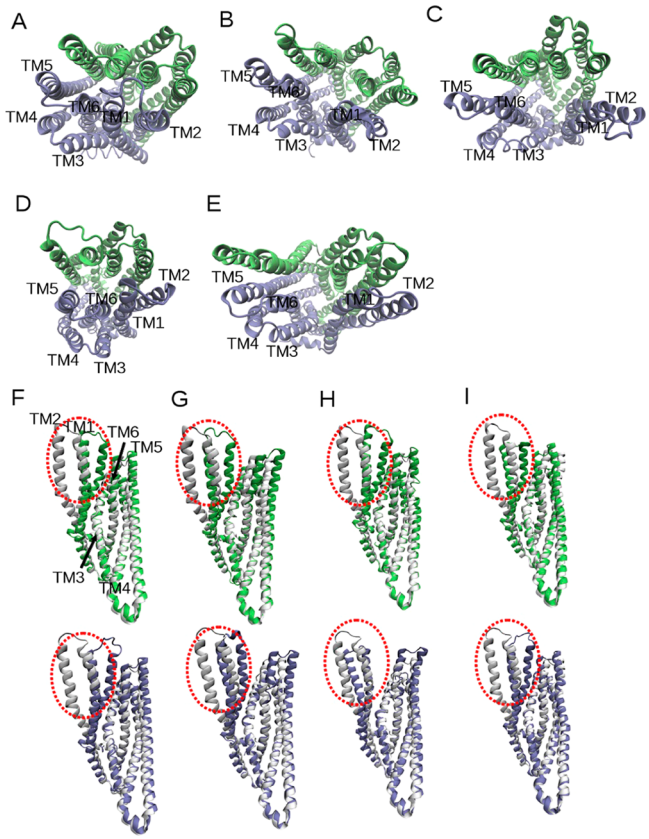

Figure 5. Structural comparisons of the outward-facing state obtained in the simulations and the outward-facing homology model of McjD based on Sav1866. Top view of the (A) occluded crystal structure, the outward-facing structures of (B) Figures 2, (C) Figure 3, and (D) Figure 4, and the (E) outward-facing McjD homology model. Superimposition of the (F) occluded structure and the outward-facing structures of (G) Figures 2, (H) Figure 3, and (I) Figure 4 with the outward facing homology model, respectively. The last conformation of the simulations in Figure 2−4 was used for structural comparisons. Only the TMDs are shown for clarity. Chain A and chain B are shown in green and blue, respectively in panels A−E. In panels F−I, chain A and chain B of the occluded structure, the outward-facing structures of Figures 2, 3, and 4 are shown in green and blue, respectively, whereas both chains of the outward-facing homology model are shown in gray.

We also calculated the distances between the centers of mass of ECL1 and ECL3 (extracellular loop 3, the loop connecting TM5 and TM6) of the same subunit and the distances between ECL1 of one subunit and ECL3 of the opposite subunit, respectively. These distances could be used as a measure of the contacts and interactions between the transmembrane helices at the extracellular side and gives an idea of how these helices change their conformation in different states. The distances between ECL1 of chain A and ECL3 of chain B are similar for the three states in Figure 6, ranging from 1.2 to 1.4 nm. However, the distances between ECL1 and ECL3 of the same subunit are 2.2, 3.9, and 3.0 nm for the occluded state, the outward-facing homology model and the outward-facing state in simulation (Figure 6A-C). These distances imply that TM1 and 2, while shifted away from TM5 and 6 of the same subunit, still interact with TM5 and 6 of the opposite subunit. These distances show that, the outward-facing state observed in the simulations opens to a lesser extent than the outward-facing

DOI: 10.1021/acs.biochem.5b00753
Biochemistry 2015, 54, 5989−5998

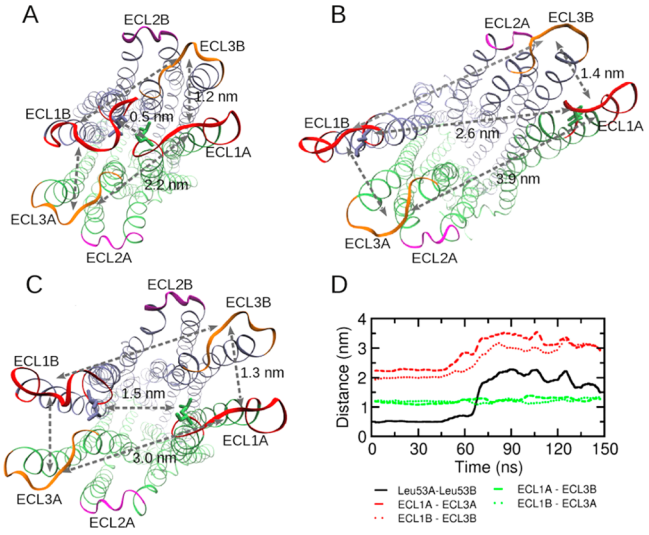

Figure 6. Distances between the extracellular loops (ECLs) of McjD. (A) The occluded state; (B) the outward-facing homology model; (C) the outward-facing state obtained by the simulation in Figure 2; (D) distances in the simulations in Figure 2 as a function of simulation time. The values are running averages of 5 ns. Chain A and chain B are shown in green and blue, respectively. ECL1 (loop between TM1 and TM2), ECL2 (loop between TM3 and TM4), and ECL3 (loop between TM5 and TM6) are shown in red, magenta, and orange, respectively. Leu53 is shown in green for chain A and blue for chain B. The distances between Leu53 residues, as well as the distances between ECL1 and ECL3 of the same subunit and from adjacent subunits are labeled.

homology model, consistent with the change in distance between the Leu53 residues. We also show these distances for simulations in Figure 2 as a function of time in Figure 6D. The distances between the Leu53 residues of the two monomers and the distances between ECL1 of one subunit and ECL3 of the opposite subunit increased during ca. 60−90 ns, indicating conformational changes. This is consistent with the RMSD values in Figure 2C and structural overlaps in Figure 2D, which also implied conformational changes during ca. 60−90 ns.

As a consistency test and to increase statistics, we performed five replicas of the same simulation with the same pull rate (4×10^{-5} nm/ps) and force constant (2000 kJ/(mol nm^2)) but with different initial velocities. This set of simulations reproduced the smaller extracellular opening observed with the first simulation (Figures S6−S8).

An interesting feature of the opening motion described by some of the simulations is that the conformational changes are asymmetrical, and mainly affect only one of the two halves of the transporter, as shown by the RMSD values of Figures S6−S8. For instance, in Simulation 4 (Figure S8), the RMSD of chain A stabilized at ca. 0.2 nm, whereas the RMSD value of chain B increased to ca. 0.5 nm after ca. 100 ns of simulation time, suggesting different conformational changes in the two subunits. This may be related to the asymmetrical structure of McjJ25. Despite the asymmetrical conformational changes, the motions of the TM helices in Simulation 4 were similar to those found in Simulation 1 of Figure 2, i.e., TM helices 1 and 2 contributed most to the transporter opening. In addition, after McjJ25 release, the transporter maintained the outward-facing state in two out of six simulations (Simulations 1 and 2 in Group 2 in Table 1, Figure 2 and Figure S6), whereas in the other simulations, during the last 35 ns, it reverted toward the initial occluded state (Figures S7−8). This observation may support the hypothesis suggested by the McjD crystal structure,[8] according to which upon release of the ligand, the transporter adopts a nucleotide-bound outward occluded conformation before reverting to an inward-facing conformation. However, we cannot rule out that the reversion to the initial occluded state is a response of the protein to the nonequilibrium process we subject it to. This is impossible to test conclusively by further simulations.

Equilibrium Simulations Starting from Different Points from the Nonequilibrium Trajectories. In order to further investigate the structural changes revealed by the previously described set of simulations, we used the structure of the McjJ25-McjD complex at 50 ns of the simulation in Figure 2 as input structure for additional 500 ns simulations, carried out with a 10-fold slower pull rate (4×10^{-6} nm/ps) (Figure 3, Simulations of Group 3 in Table 1).

The conformational changes of the two TMDs that occurred in this simulation are asymmetric (Figure 3C), and somewhat larger than the original simulation in Figure 2 (RMSD values of 0.4 and 0.3 nm, respectively). The conformational changes mainly affected one-half of the transporter (namely, chain B), whereas the other half remained almost unchanged (RMSD values for the two chains are ca. 0.5 and 0.2 nm, as shown in Figure 3C and E). As shown in Figure 3D and Figure 5H, the conformational changes of TM1 and 2 are larger than those shown in Figure 2. However, the overall degree of opening of the dimer is still smaller than the outward-facing homology model. Here, toward the end of the simulation, the force decreased to 100 kJ/(mol nm), suggesting that the transporter reached an extracellular opening that allows ligand release, as we found in the simulations in Figure 2. The simulation was repeated three times with reproducible results and force profiles.

Additional simulations were also carried out to validate the conformational changes in the transporter shown in Figure 2. For this set of simulations (Group 4 in Table 1, Figure 4), the initial structure, the pull rate (4×10^{-5} nm/ps), and the force constant (2000 kJ/(mol nm^2)) were the same as those used for the simulations shown in Figure 2. However, here, the system was equilibrated at each force maximum for 150 ns, so that the process of conformational changes was sampled more extensively.

In this simulation, the RMSD values of TMDs increased gradually during the pulling (Figure 4C and Figure S9), while for the simulation in Figure 2 both the increase of RMSD values and conformational changes happened quickly when the force reached the maximum value (in between ca. 60−90 ns). Overall, the structural changes are comparable with those of the simulations in Figure 2, with RMSD values of ca. 0.3 nm (Figure 4D and Figure 5A−E), slightly smaller than those in Figure 3. In both of the simulations in Figure 3 and 4, the structural changes mainly occurred within TM1 and TM2, consistent with the results in Figure 2 (Figure 5H−J).

DISCUSSION

Protein dynamics involves different type of motions, ranging from displacement of single atoms to domain motions, with a time-scale for large conformational changes in the range of milliseconds to seconds.[47,48] MD simulations have extensively been used to investigate protein dynamics,[49,50] reaching, especially for smaller proteins, time-scales that are of biological relevance.[51] Nonequilibrium MD simulations are also used to

DOI: 10.1021/acs.biochem.5b00753
Biochemistry 2015, 54, 5989−5998

investigate conformational changes of large systems that are too slow to sample directly by equilibrium simulations. An important example is a set of simulations on the ABC transporter MsbA in which a number of possible pathways defined by collective motions of domains was systematically investigated by steered molecular dynamics.[15] Here, we used a simpler reaction coordinate to induce the translocation from the cavity of McjD to the extracellular side of MccJ25. The exact time scale for this event is not known experimentally but it likely very much longer than the microsecond time scale that can be reached by atomistic simulations. We make use of the relatively large size of the substrate to investigate the range of motions of McjD in response to the forced motion of the ligand MccJ25. To release the substrate on the extracellular side, the transporter has to switch to an outward-facing state. By monitoring the protein conformational changes during this process, we attempt to infer the extent of the conformational changes associated with MccJ25 transport and release from the cavity.

Limitations and Validation of Nonequilibrium Simulations. The pull simulations in this study have several limitations that should be considered carefully in order to interpret the conformational changes revealed by these simulations. First, the pull simulations were started from a structure of the MccJ25/McjD complex created by manually docking MccJ25 in the cavity of McjD as described in the Methods section. The simulations cannot exhaustively sample the interactions between MccJ25 and the residues in the binding cavity, either before or during the pull process, and therefore specific interactions between the peptide and the transporter are not worth analyzing in detail. In addition, the initial configuration of MccJ25 may affect the exact conformational changes during the pulling process. However, we do think it is unlikely that the initial binding configuration of MccJ25 would affect the degree of the transporter opening to the extracellular side. The simulations are designed to give a qualitative picture of the scale of the conformational changes in the transporter associated with transport.

Second, in all of the simulations, MccJ25 was pulled along one pathway (the Z axis), suggested by the general symmetry of ABC transporters. The peptide was free to move in the X and Y plane at the same time, but this is limited by the pull rate. It is possible that the substrate could follow a different, more convoluted path. This is a general concern with simulations that, by necessity, explore a specific reaction coordinate.

A third limitation is the pull rate. As mentioned in the Results, the pull rates used in this study are based on a compromise between computational feasibility, expected time scales of conformational changes in the transporter, and perhaps the peptide, and changes in the interactions between the peptide and the transporter. At high pull rates, much of the work done by the pull force will result in nonequilibrium work due to friction, causing heat, which is dissipated in the system and removed by coupling to a thermostat. At very low rates, in the ideal case, the system will be in equilibrium at every point along the path and the pull force will reflect the underlying thermodynamic energy landscape. The actual simulations are somewhere in between, but contain a significant amount of nonequilibrium work and the resulting energies cannot yet be interpreted as free energy profiles. However, three different pull rates ranging from 1×10^{-4} to 4×10^{-6} kJ/(mol nm^2) (Table 1) are employed in our studies, and they all resulted in comparable pull force profiles and similar degrees of transporter opening to the extracellular side (Figures 2−4). This indicates that the necessary changes in McjD conformation for MccJ25 release are independent of the pull rates, and are likely to be similar at much slower rates.

Range of Conformational Changes during the Transport Cycle. As described in the Results section, the outward-facing structures observed in our simulation suggest a degree of opening of the TMDs that is significantly smaller than the opening of the outward-facing state of Sav1866[9] (Figure 5). For simulations in Figure 2 and 4, the conformational changes in both chains are smaller than those of the outward-facing homology model (Figure 5G,I). For simulations in Figure 3, the changes in chain B are comparable with those suggested by the outward-facing homology model, but chain A remained almost unchanged (Figure 5H). Thus, the overall transporter structure also opened to a lesser extent compared to the outward-facing homology model.

Structural superimposition of both the outward-facing structure extracted from MD simulations (Figures 2−4) and the homology model (Figure 5F) based on Sav1866 with the occluded crystal structure showed that TM1 and 2 undergo more significant conformational changes than the other helices, suggesting that these helices play a role in driving the transporter opening at the extracellular side. In all of the structures in Figure 5B−E, TM1 and 2 are shifted away from the other helices of the same subunit, while maintaining the interactions between them and TM5 and 6 of the opposite subunit. Overall, the structures obtained from our MD simulations suggest conformational changes consistent with the outward-facing homology model, but with a smaller magnitude.

Simulations in Figure 2 resulted in an outward-facing structure with symmetrical conformational changes of both subunits. Figure 6 shows the distances between residues and loops at the extracellular side for this less open outward-facing structure, the outward-facing homology model, and the occluded crystal structure. The distances between the Leu53 residues in the outward-facing conformation (Figure 2) and the homology model are 1.0 and 2.1 nm larger than that of the occluded structure, respectively. The distances between ECL1 and ECL3 from the same subunit in these two outward-facing structures are 0.8 and 1.7 nm larger than the corresponding values in the occluded structure. Overall, in the MD simulations, McjD opens to the extracellular side roughly half of the extent observed in the homology model. The other simulations resulted in somewhat different outward-facing structures (e.g., Figures S6−S8 and Figure 3 show asymmetrical conformations), but with a comparable degree of transporter opening. The differences between the outward-facing structures from MD simulations with different protocols and the outward-facing homology model are significant.

Several crystal structures of ABC exporters[10,52−57] have been solved in inward-facing states characterized by different orientation and different degrees of separation between the NBDs. For example, Ward et al.[10] reported two inward-facing crystal structures for MsbA. In one of the structures, the two NBDs establish contacts with each other (PDB ID: 3B5X), whereas the two NBDs are separated in the other structure (PDB ID: 3B5W). Shintre et al.[56] showed structures of ABCB10, for the apo form and the complex with ATP analogs, characterized by slightly different intracellular opening. Ward et al.[57] also reported three different inward-facing structures for P-glycoprotein (P-gp) with small changes in the separation

DOI: 10.1021/acs.biochem.5b00753
Biochemistry 2015, 54, 5989−5998

between the NBDs. Overall, these structures show an intracellular opening larger than the P-gp crystal structure reported by Aller et al.[52] In addition, EPR spectroscopy and MD simulations[22] revealed intrinsic large flexibility for P-gp by showing broad distributions of the distance between the NBDs. Although the flexibility revealed by the experimental and theoretical studies mentioned above is for inward-facing states and we are aware that the inward-facing and the outward-facing states are different putative intermediate structures likely associated with different dynamic properties, our results suggest that the outward-facing state may also have some degree of flexibility.

There are only two outward-facing crystal structures reported for ABC exporters, for MsbA and Sav1866,[9,10] which adopt a very similar conformation. The opening of these structures at the extracellular side is larger than that found in our MD simulations, as discussed above. However, many outward-facing structures have been solved for ABC importers, and indicate a much more limited extent of opening.[58−60] For instance, Figure 7 shows the transmembrane domains of the outward-facing conformation of the maltose transporter (PDB ID: 2R6G).[60] The distances between residues at the extracellular side of the TM helices indicate a much smaller opening compared with the outward-facing state of Sav1866 and MsbA. The simulations of McjD suggest a similar scale (Figure 7).

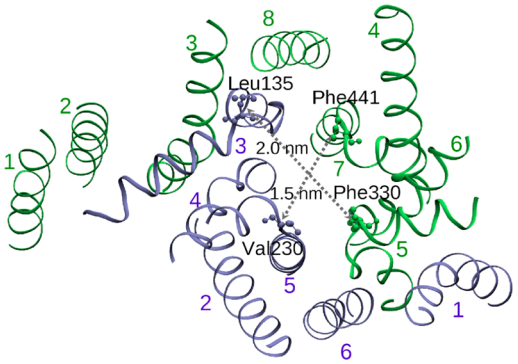

Figure 7. Distances between residues at the extracellular side of transmembrane helices of the maltose importer. MalF and MalG are shown in light green and light blue, respectively. Phe330 of TM 5 and Phe441 of TM7 from MalF are shown in ball and stick model in light green, whereas Leu135 of TM3 and Val230 of TM5 from MalG are shown in ball and stick model in light blue. The distance between Phe330 and Leu135, as well as the distance between Phe441 and Val230 are labeled.

CONCLUSIONS

Using a combination of equilibrium and nonequilibrium MD simulations, we investigated the conformational changes of the ABC transporter McjD following MccJ25 translocation and release to the extracellular side. Our simulations revealed a limited range of transporter opening, thus suggesting that the larger extracellular separation among the TM helices observed in crystal structures of ABC exporters might not be necessary functionally. MccJ25 is a large substrate, which suggests that the range of motions might even be less for smaller substrates.

ASSOCIATED CONTENT

Supporting Information

The Supporting Information is available free of charge on the ACS Publications website at DOI: 10.1021/acs.biochem.5b00753.

Sequence alignment of the TMDs (Figure S1) and NBDs (Figure S2) of ABC transporters. Pull force profiles (Figure S3), positions of MccJ25 relative to the protein (Figure S4), and RMSD values of TMDs (Figure S5) based on simulations in Group 1 in Table 1. Conformational changes of McjD based on Simulations 2 (Figure S6) and 3 (Figure S7) in Group 2 in Table 1. Pull force profiles, positions of MccJ25 relative to the protein, and RMSD values of TMDs (Figure S8) based on simulations 4−6 in Group 2 in Table 1. RMSD values of TMDs of each equilibrium simulation (Figure S9) in Group 4 in Table 1 (PDF)

AUTHOR INFORMATION

Corresponding Author

*E-mail: tieleman@ucalgary.ca.

Present Address

#(H.G.C.) Institute for Molecular Bioscience, The University of Queensland, St Lucia, QLD 4072, Australia.

Funding

D.P.T. is the Alberta Innovates Technology Futures Strategic Chair in (Bio)Molecular Simulation and an Alberta Innovates Health Solutions (AIHS) Scientist. R.X.G. is supported by postdoctoral fellowships from the CREATE Training Program in Bionanomachines, Canadian Institutes for Health Research (CIHR, funding reference number: MFE-140949), and AIHS. This work was supported by CIHR (MOP-62690).

Notes

The authors declare no competing financial interest.

ACKNOWLEDGMENTS

Calculations were carried out in part on WestGrid/Compute Canada facilities.

REFERENCES

(1) Holland, I. B., Cole, S. P., Kuchler, K., and Higgins, C. F. (2003) *ABC Proteins: from Bacteria to Man*; 1st Edition, Academic Press, New York.

(2) Hinz, A., and Tampé, R. (2012) ABC transporters and immunity: mechanism of self-defense. *Biochemistry 51*, 4981−4989.

(3) Tarling, E. J., de Aguiar Vallim, T. Q., and Edwards, P. A. (2013) Role of ABC transporters in lipid transport and human disease. *Trends Endocrinol. Metab. 24*, 342−350.

(4) Aittoniemi, J., Fotinou, C., Craig, T. J., de Wet, H., Proks, P., and Ashcroft, F. M. (2009) SUR1: a unique ATP-binding cassette protein that functions as an ion channel regulator. *Philos. Trans. R. Soc., B 364*, 257−267.

(5) Gadsby, D. C., Vergani, P., and Csanády, L. (2006) The ABC protein turned chloride channel whose failure causes cystic fibrosis. *Nature 440*, 477−483.

(6) Fletcher, J. I., Haber, M., Henderson, M. J., and Norris, M. D. (2010) ABC transporters in cancer: more than just drug efflux pumps. *Nat. Rev. Cancer 10*, 147−156.

(7) Gottesman, M. M., Fojo, T., and Bates, S. E. (2002) Multidrug resistance in cancer: role of ATP−dependent transporters. *Nat. Rev. Cancer. 2*, 48−58.

(8) Choudhury, H. G., Tong, Z., Mathavan, I., Li, Y., Iwata, S., Zirah, S., Rebuffat, S., van Veen, H. W., and Beis, K. (2014) Structure of an

DOI: 10.1021/acs.biochem.5b00753
Biochemistry 2015, 54, 5989−5998

antibacterial peptide ATP-binding cassette transporter in a novel outward occluded state. *Proc. Natl. Acad. Sci. U. S. A. 111*, 9145−9150.
(9) Dawson, R. J., and Locher, K. P. (2006) Structure of a bacterial multidrug ABC transporter. *Nature 443*, 180−185.
(10) Ward, A., Reyes, C. L., Yu, J., Roth, C. B., and Chang, G. (2007) Flexibility in the ABC transporter MsbA: Alternating access with a twist. *Proc. Natl. Acad. Sci. U. S. A. 104*, 19005−19010.
(11) Becker, J.-P., Van Bambeke, F., Tulkens, P. M., and Prévost, M. (2010) Dynamics and structural changes induced by ATP binding in SAV1866, a bacterial ABC exporter. *J. Phys. Chem. B 114*, 15948−15957.
(12) George, A. M., and Jones, P. M. (2013) An asymmetric post-hydrolysis state of the ABC transporter ATPase dimer. *PLoS One 8*, e59854.
(13) Jones, P. M., and George, A. M. (2007) Nucleotide-dependent Allostery within the ABC Transporter ATP-binding Cassette A COMPUTATIONAL STUDY OF THE MJ0796 DIMER. *J. Biol. Chem. 282*, 22793−22803.
(14) Kandt, C., and Tieleman, D. P. (2010) Holo-BtuF stabilizes the open conformation of the vitamin B12 ABC transporter BtuCD. *Proteins: Struct., Funct., Genet. 78*, 738−753.
(15) Moradi, M., and Tajkhorshid, E. (2013) Mechanistic picture for conformational transition of a membrane transporter at atomic resolution. *Proc. Natl. Acad. Sci. U. S. A. 110*, 18916−18921.
(16) O'Mara, M. L., and Mark, A. E. (2012) The effect of environment on the structure of a membrane protein: P-glycoprotein under physiological conditions. *J. Chem. Theory Comput. 8*, 3964−3976.
(17) O'Mara, M. L., and Mark, A. E. (2014) Structural characterization of two metastable ATP-bound states of P-glycoprotein. *PLoS One 9*, e91916.
(18) Oliveira, A. S., Baptista, A. M., and Soares, C. M. (2011) Conformational changes induced by ATP-hydrolysis in an ABC transporter: A molecular dynamics study of the Sav1866 exporter. *Proteins: Struct., Funct., Genet. 79*, 1977−1990.
(19) Oloo, E. O., Kandt, C., O'Mara, M. L., and Tieleman, D. P. (2006) Computer simulations of ABC transporter components. *Biochem. Cell Biol. 84*, 900−911.
(20) Wen, P.-C., and Tajkhorshid, E. (2008) Dimer opening of the nucleotide binding domains of ABC transporters after ATP hydrolysis. *Biophys. J. 95*, 5100−5110.
(21) Wen, P.-C., and Tajkhorshid, E. (2011) Conformational coupling of the nucleotide-binding and the transmembrane domains in ABC transporters. *Biophys. J. 101*, 680−690.
(22) Wen, P.-C., Verhalen, B., Wilkens, S., Mchaourab, H. S., and Tajkhorshid, E. (2013) On the origin of large flexibility of P-glycoprotein in the inward-facing state. *J. Biol. Chem. 288*, 19211−19220.
(23) Weng, J.-W., Fan, K.-N., and Wang, W.-N. (2012) The conformational transition pathways of ATP-binding cassette transporter BtuCD revealed by targeted molecular dynamics simulation. *PLoS One 7*, e30465.
(24) Weng, J.-W., Fan, K.-N., and Wang, W.-N. (2010) The conformational transition pathway of ATP binding cassette transporter MsbA revealed by atomistic simulations. *J. Biol. Chem. 285*, 3053−3063.
(25) van Wonderen, J. H., McMahon, R. M., O'Mara, M. L., McDevitt, C. A., Thomson, A. J., Kerr, I. D., MacMillan, F., and Callaghan, R. (2014) The central cavity of ABCB1 undergoes alternating access during ATP hydrolysis. *FEBS J. 281*, 2190−2201.
(26) Rebuffat, S., Blond, A., Destoumieux-Garzón, D., Goulard, C., and Peduzzi, J. (2004) Microcin J25, from the macrocyclic to the lasso structure: implications for biosynthetic, evolutionary and biotechnological perspectives. *Curr. Protein Pept. Sci. 5*, 383−391.
(27) Rosengren, K. J., Clark, R. J., Daly, N. L., Göransson, U., Jones, A., and Craik, D. J. (2003) Microcin J25 has a threaded sidechain-to-backbone ring structure and not a head-to-tail cyclized backbone. *J. Am. Chem. Soc. 125*, 12464−12474.
(28) Hess, B., Kutzner, C., Van Der Spoel, D., and Lindahl, E. (2008) GROMACS 4: algorithms for highly efficient, load-balanced, and scalable molecular simulation. *J. Chem. Theory Comput. 4*, 435−447.
(29) Pronk, S., Páll, S., Schulz, R., Larsson, P., Bjelkmar, P., Apostolov, R., Shirts, M. R., Smith, J. C., Kasson, P. M., van der Spoel, D., Hess, B., and Lindahl, E. (2013) GROMACS 4.5: a high-throughput and highly parallel open source molecular simulation toolkit. *Bioinformatics 29*, 845−854.
(30) Lindorff-Larsen, K., Piana, S., Palmo, K., Maragakis, P., Klepeis, J. L., Dror, R. O., and Shaw, D. E. (2010) Improved side-chain torsion potentials for the Amber ff99SB protein force field. *Proteins: Struct., Funct., Genet. 78*, 1950−1958.
(31) Jämbeck, J. P., and Lyubartsev, A. P. (2012) Derivation and systematic validation of a refined all-atom force field for phosphatidylcholine lipids. *J. Phys. Chem. B 116*, 3164−3179.
(32) Jämbeck, J. P., and Lyubartsev, A. P. (2012) An extension and further validation of an all-atomistic force field for biological membranes. *J. Chem. Theory Comput. 8*, 2938−2948.
(33) Jämbeck, J. P., and Lyubartsev, A. P. (2013) Another piece of the membrane puzzle: extending slipids further. *J. Chem. Theory Comput. 9*, 774−784.
(34) Meagher, K. L., Redman, L. T., and Carlson, H. A. (2003) Development of polyphosphate parameters for use with the AMBER force field. *J. Comput. Chem. 24*, 1016−1025.
(35) Darden, T., York, D., and Pedersen, L. (1993) Particle mesh Ewald: An N·log (N) method for Ewald sums in large systems. *J. Chem. Phys. 98*, 10089−10092.
(36) Essmann, U., Perera, L., Berkowitz, M. L., Darden, T., Lee, H., and Pedersen, L. G. (1995) A smooth particle mesh Ewald method. *J. Chem. Phys. 103*, 8577−8593.
(37) Bussi, G., Donadio, D., and Parrinello, M. (2007) Canonical sampling through velocity rescaling. *J. Chem. Phys. 126*, 014101.
(38) Nosé, S. (1984) A molecular dynamics method for simulations in the canonical ensemble. *Mol. Phys. 52*, 255−268.
(39) Parrinello, M., and Rahman, A. (1981) Polymorphic transitions in single crystals: A new molecular dynamics method. *J. Appl. Phys. 52*, 7182−7190.
(40) Wolf, M. G., Hoefling, M., Aponte-Santamaría, C., Grubmüller, H., and Groenhof, G. (2010) g_membed: Efficient insertion of a membrane protein into an equilibrated lipid bilayer with minimal perturbation. *J. Comput. Chem. 31*, 2169−2174.
(41) Jorgensen, W. L., Chandrasekhar, J., Madura, J. D., Impey, R. W., and Klein, M. L. (1983) Comparison of simple potential functions for simulating liquid water. *J. Chem. Phys. 79*, 926−935.
(42) Neria, E., Fischer, S., and Karplus, M. (1996) Simulation of activation free energies in molecular systems. *J. Chem. Phys. 105*, 1902−1921.
(43) Corradi, V., Singh, G., and Tieleman, D. P. (2012) The Human Transporter Associated with Antigen Processing MOLECULAR MODELS TO DESCRIBE PEPTIDE BINDING COMPETENT STATES. *J. Biol. Chem. 287*, 28099−28111.
(44) Katoh, K., Misawa, K., Kuma, K. i., and Miyata, T. (2002) MAFFT: a novel method for rapid multiple sequence alignment based on fast Fourier transform. *Nucleic Acids Res. 30*, 3059−3066.
(45) Šali, A., and Blundell, T. L. (1993) Comparative protein modelling by satisfaction of spatial restraints. *J. Mol. Biol. 234*, 779−815.
(46) Dawson, R. J., and Locher, K. P. (2007) Structure of the multidrug ABC transporter Sav1866 from Staphylococcus aureus in complex with AMP-PNP. *FEBS Lett. 581*, 935−938.
(47) Dror, R. O., Jensen, M. Ø., Borhani, D. W., and Shaw, D. E. (2010) Exploring atomic resolution physiology on a femtosecond to millisecond timescale using molecular dynamics simulations. *J. Gen. Physiol. 135*, 555−562.
(48) Grant, B. J., Gorfe, A. A., and McCammon, J. A. (2010) Large conformational changes in proteins: signaling and other functions. *Curr. Opin. Struct. Biol. 20*, 142−147.

DOI: 10.1021/acs.biochem.5b00753
Biochemistry 2015, 54, 5989−5998

(49) Klepeis, J. L., Lindorff-Larsen, K., Dror, R. O., and Shaw, D. E. (2009) Long-timescale molecular dynamics simulations of protein structure and function. *Curr. Opin. Struct. Biol. 19*, 120−127.
(50) Shaw, D. E., Maragakis, P., Lindorff-Larsen, K., Piana, S., Dror, R. O., Eastwood, M. P., Bank, J. A., Jumper, J. M., Salmon, J. K., Shan, Y., and Wriggers, W. (2010) Atomic-level characterization of the structural dynamics of proteins. *Science 330*, 341−346.
(51) Zwier, M. C., and Chong, L. T. (2010) Reaching biological timescales with all-atom molecular dynamics simulations. *Curr. Opin. Pharmacol. 10*, 745−752.
(52) Aller, S. G., Yu, J., Ward, A., Weng, Y., Chittaboina, S., Zhuo, R., Harrell, P. M., Trinh, Y. T., Zhang, Q., Urbatsch, I. L., and Chang, G. (2009) Structure of P-glycoprotein reveals a molecular basis for poly-specific drug binding. *Science 323*, 1718−1722.
(53) Hohl, M., Briand, C., Grütter, M. G., and Seeger, M. A. (2012) Crystal structure of a heterodimeric ABC transporter in its inward-facing conformation. *Nat. Struct. Mol. Biol. 19*, 395−402.
(54) Jin, M. S., Oldham, M. L., Zhang, Q., and Chen, J. (2012) Crystal structure of the multidrug transporter P-glycoprotein from Caenorhabditis elegans. *Nature 490*, 566−569.
(55) Kodan, A., Yamaguchi, T., Nakatsu, T., Sakiyama, K., Hipolito, C. J., Fujioka, A., Hirokane, R., Ikeguchi, K., Watanabe, B., Hiratake, J., Kimura, Y., Suga, H., Ueda, K., and Kato, H. (2014) Structural basis for gating mechanisms of a eukaryotic P-glycoprotein homolog. *Proc. Natl. Acad. Sci. U. S. A. 111*, 4049−4054.
(56) Shintre, C. A., Pike, A. C., Li, Q., Kim, J.-I., Barr, A. J., Goubin, S., Shrestha, L., Yang, J., Berridge, G., Ross, J., et al. (2013) Structures of ABCB10, a human ATP-binding cassette transporter in apo-and nucleotide-bound states. *Proc. Natl. Acad. Sci. U. S. A. 110*, 9710−9715.
(57) Ward, A. B., Szewczyk, P., Grimard, V., Lee, C.-W., Martinez, L., Doshi, R., Caya, A., Villaluz, M., Pardon, E., Cregger, C., et al. (2013) Structures of P-glycoprotein reveal its conformational flexibility and an epitope on the nucleotide-binding domain. *Proc. Natl. Acad. Sci. U. S. A. 110*, 13386−13391.
(58) Korkhov, V. M., Mireku, S. A., Veprintsev, D. B., and Locher, K. P. (2014) Structure of AMP-PNP−bound BtuCD and mechanism of ATP-powered vitamin B12 transport by BtuCD−F. *Nat. Struct. Mol. Biol. 21*, 1097−1099.
(59) Oldham, M. L., and Chen, J. (2011) Snapshots of the maltose transporter during ATP hydrolysis. *Proc. Natl. Acad. Sci. U. S. A. 108*, 15152−15156.
(60) Oldham, M. L., Khare, D., Quiocho, F. A., Davidson, A. L., and Chen, J. (2007) Crystal structure of a catalytic intermediate of the maltose transporter. *Nature 450*, 515−521.

DOI: 10.1021/acs.biochem.5b00753
Biochemistry 2015, 54, 5989−5998